Hindcasts of tropical Atlantic SST gradient and South American precipitation: the influences of the ENSO forcing and the Atlantic preconditioning

Huei-Ping Huang[1], Andrew W. Robertson[2], Yochanan Kushnir[1], Shiling Peng[3]

[1] *Lamont-Doherty Earth Observatory of Columbia University*
[2] *International Research Institute for Climate and Society, Columbia University*
[3] *NOAA ESRL/Physical Science Division and CIRES, University of Colorado*

April 2008

Abstract

Hindcast experiments for the tropical Atlantic sea surface temperature (SST) gradient, G1, defined as tropical North Atlantic SST anomaly minus tropical South Atlantic SST anomaly, are performed using an atmospheric general circulation model coupled to a mixed-layer ocean over the Atlantic to quantify the contributions of the El Nino-Southern Oscillation (ENSO) forcing and the preconditioning in the Atlantic to G1 in boreal spring. The results confirm previous observational analyses that in the years with a persistent ENSO SST anomaly from boreal winter to spring, the ENSO forcing plays a primary role in determining the tendency of G1 from winter to spring and the sign of G1 in late spring. In the hindcasts, the initial perturbations in Atlantic SST in boreal winter are found to generally persist beyond a season, leaving a secondary but non-negligible contribution to the predicted Atlantic SST gradient in spring. For 1993-94, a neutral year with a large pre-existing G1 in winter, the hindcast using the information of Atlantic preconditioning alone is found to reproduce the observed G1 in spring. The seasonal predictability in precipitation over South America is examined in the hindcast experiments. For the recent events that can be validated with high-quality observations, the hindcasts produced dryness in boreal Spring 1983, wetness in Spring 1996, and wetness in Spring 1994 over northern Brazil that are qualitatively consistent with observations. An inclusion of the Atlantic preconditioning is found to help the prediction of South American rainfall in boreal spring. For the ENSO years, discrepancies remain between the hindcast and observed precipitation anomalies over the northern and equatorial South America, an error that is partially attributed to the biased atmospheric response to ENSO forcing in the model. The hindcast of the 1993-94 neutral year does not suffer this error. It constitutes an intriguing example of useful seasonal forecast of G1 and South American rainfall anomalies without ENSO.

1. Introduction

The research in the predictability of tropical Atlantic meridional SST gradient has a long history since early studies suggested its potential influences on the rainfall anomaly over the Nordeste (northern Brazil) region of South America (e.g., Nobre and Molion 1988, see the survey in Uvo et al. 1998). Using station data for precipitation, previous observational analyses (e.g., Giannini et al. 2004) showed that, in boreal spring, the Nordeste region tends to be drier than normal with a positive Atlantic SST gradient, G1 (defined as tropical North Atlantic SST anomaly (tNA) minus tropical South Atlantic SST anomaly (tSA)), because a warmer than normal tNA or a colder than normal tSA drives the Atlantic ITCZ northward, away from the Nordeste. Conversely, a negative G1 implies wetness over northern Brazil. This suggests the possibility of incorporating the prediction of G1 in the practical prediction of the rainfall anomalies over South America.

Among the two components of SSTs that define G1, tNA is known to be more strongly influenced by ENSO and is positively correlated with the NINO3 SST index (e.g., Enfield and Mayer 1997, Alexander and Scott 2002, Huang et al. 2005a), while tSA is recognized as being regulated by local internal variability (e.g., Chang et al. 1998, Czaja et al. 2002, Trzaska et al. 2007). Thus, G1 tends to have the same sign as the NINO3 index in the boreal spring of "year 1" of a strong ENSO event after the influence of ENSO on the Atlantic is fully established. Using the observation from 1876-1997, Huang et al. (2005a) clarified that about two-third of the strong ENSO events are concordant, in the sense (as defined by Giannini et al. 2004) that G1 in boreal spring has the same sign as the NINO3 index averaged from the preceding winter to early spring. The other one-third are discordant, for which the ENSO forcing from boreal winter to spring is not sufficient to overturn a pre-existing Atlantic SST gradient such that G1 and NINO3 have opposite signs in spring. In the discordant cases, tSA in boreal spring can often be tracked back to a strong pre-existing SST anomaly in the central South Atlantic in the preceding boreal winter (Huang et al. 2005a, Barreiro et al. 2004). Figure 1, adapted from Huang et al. (2005a), illustrates the composites of the SST anomalies for the (a) concordant, and (b) discordant cases, and (c) the typical precondition for the latter. Following previous work (Giannini et al. 2004, Huang et al. 2005a), the two boxes in Fig. 1a are chosen to define the tNA and tSA used in this study. Based on the observational analysis, G1 in boreal spring should generally depend on the ENSO forcing from boreal winter to spring and the preconditioning in the Atlantic SST in boreal winter. In this study, we will use a series of GCM hindcast experiments to assess the contributions of these two components to the seasonal predictability in the Atlantic SST and in the precipitation over South America.

We will analyze the behavior of the simulated SST anomalies in ensemble hindcast experiments using an atmospheric GCM partially coupled to a mixed-layer ocean model for the Atlantic. The experimental design is described in Section 2. The results of the model simulations of the Atlantic SST and SST gradient are discussed in Section 3. In addition to the SST, the model predicted precipitation anomalies will be analyzed in Section 4 in the context of the relationships among the Atlantic SST gradient, ENSO forcing, and South American rainfall anomalies. Concluding remarks follow in Section 5.

2. The model and numerical experiments

2a. Selection of cases

We will focus on selected years with the combinations of one or more of the following conditions: (i) Persistent ENSO forcing from boreal winter to spring; (ii) A strong preconditioning in the Atlantic SST in boreal winter; (iii) A large tendency in, or strong persistence of, G1 from boreal winter to spring. These criteria are quantified by the monthly NINO3 and G1 indices as shown in Fig. 2. They are detrended in time in the same manner as in Huang et al. (2005a). Each grid box represents one month and each row in one of the panels in Fig. 2, from left to right, represents one year, defined as July of one year (called "year 0") to June of the following year (called "year 1"), with time increasing downward from 1947 to 1997 (the top row is July 1947-June 1948, bottom row is July 1996-June 1997.) Note that the color interval, shown at bottom, for G1 is only on-third of that for NINO3. Visually, the right panel looks noisier than the left panel; The NINO3 index exhibits a greater degree of month-to-month persistence. However, the persistence of NINO3 is stronger in the first half (from boreal summer of yr 0 to winter of yr 0/1) of the ENSO year, leaving us a reduced number of cases with the desired condition of a persistent ENSO forcing from boreal winter to spring of yr 1, the time of year when G1 is important. Among these cases, a few are found to have a large tendency (or strong persistence) in G1 from boreal winter to spring. They are selected for our hindcast experiments as marked by the arrows in Fig. 2. They include two ENSO warm events (1968-69, 1982-83) and three cold events (1970-71, 1988-89, 1995-96). In addition, we selected a neutral year of 1993-94 that is distinguished by a strong preconditioning in winter and strong persistence of G1 from winter to spring. We have chosen the cases from the last 30 years of the 20th century for which there are more high-quality observational data (for Atlantic SST and precipitation) available to validate the hindcast.

2b. The model and experimental design

The hindcast model is a T42 28-level version (frozen in cir. 2001) of the National Center for Environmental Prediction (NCEP) atmospheric GCM coupled to a mixed layer ocean over the Atlantic. The mixed layer model consists of a 50 m slab ocean with "flux correction" similar to that in Peng et al. (2006) but without the Ekman transport, as detailed in Appendix A. Although the atmosphere-ocean coupling is relatively simple, there is evidence from previous studies that thermodynamic coupling alone is useful for the prediction of Atlantic SST anomalies (e.g., Giannini et al. 2004, Saravanan and Chang 2004). In multi-year test runs with climatological SST imposed outside the Atlantic, climate drift in SST is found to be small within the coupled domain. In the hindcast experiment we will use the model simulated SST minus the observed climatological SST to define the SST anomaly to be compared to observation. The domain for the mixed layer ocean model is from 50°S to 36°N over the Atlantic, as shown in Figs. 4-7. The entire South Atlantic is included because we are interested in the preconditioning in boreal winter in the South Atlantic (see Fig. 1c). Additional remarks on the detail of the mixed layer model are in Appendix A.

Each hindcast run is a one-year integration starting from a generic September 1 initial state for the atmosphere. An ensemble of 25 runs for each case are constructed by altering the atmospheric initial condition with an isotropic perturbation to the spherical harmonic components of the divergence field for total wavenumber n = 11-17 and for the vertical levels 10-14 in the middle troposphere. The atmospheric model is integrated for 2 months uncoupled and forced with climatological SST, and then coupled to the mixed-layer model on November 1 when an observed SST anomaly is imposed in the initial condition over the coupled domain. (For the convenience of execution, coupling is actually kept on during the first two months of integration but with the SST over the coupled domain restored to the seasonally varying climatological state every 12 hours when coupling is performed.) The coupled model is then integrated forward to August of year 1. For most cases, we will focus on the results from November of year 0 to June of year 1. Because the observed Atlantic SSTs have only monthly (or weekly in selected recent times) resolution, the "initial state" of SST on November 1 used in our simulation is actually taken from the average of the monthly means of October and November of the selected year.

A prototypical outcome of a prediction run with a 3-member ensemble shown in Fig. 3 serves to illustrate the behavior of the coupled model. To construct a meaningful example, the SST anomaly in the initial state in the Atlantic on November 1 is constructed from the composite of seven cases (see figure caption) that have a large, positive, SST anomaly over the South Atlantic box in Fig. 1c. Imposing the composite SST anomaly for the Atlantic in the initial condition, the three runs are performed with the climatological SST imposed outside the coupled domain. The simulated daily SST anomalies averaged over the South Atlantic box are shown in Fig. 3 with the individual ensemble members in color and the ensemble mean in black. Although the switch-on of coupling and the addition of the initial perturbation in the SST on November 1 is rather abrupt, Fig. 3 shows that, after a brief initial drop in amplitude, the model retained a substantial fraction of the initial perturbation and allowed it to persist into the spring of year 1. The filled and open circles show the monthly means of the simulated (ensemble mean) and observed (composite of the 7 selected years) SST anomalies for the South Atlantic box from November to June. The SST anomaly drops off more quickly in the model than in the observation but the former still has an e-folding time longer than a season.

Three types of runs are performed for each of the selected cases described in Section 2a. The "Initial Condition Only" (IC Only) runs are similar to the example in Fig. 3 and are performed with the observed SST anomaly imposed in the initial (November 1) state but with the seasonally varying climatological SST imposed outside the coupling domain. The "ENSO forcing Only" (ENSO Only) runs are without any initial SST perturbation on November 1 but with the observed SST anomaly over the tropical Pacific (165°E-90°W, 15°S-15°N) added to the imposed climatological SST outside the coupling domain. The ENSO+IC runs have both ENSO forcing from the Pacific and the initial perturbation in the SST over the Atlantic. (For the ENSO Only and ENSO+IC runs, during the first two months the ENSO forcing in the Pacific is already turned on.) Unless otherwise noted, each type of runs consists of a 25-member ensemble of one-year integration (i.e., total of 75 runs for each of the ENSO events described in Section 2a). In addition, a 25-member "control run" is performed with no ENSO forcing and no initial perturbation (but with coupling turned on) on November 1. This set of runs will be used to define the simulated precipitation anomalies in Section 4. Table 1 summarizes the major hindcast runs performed for this study.

3. Hindcast of SST

3a. Hindcast of Atlantic SST

Figures 4a and 4b show the observed SST anomalies over the Atlantic in November 1968 and April 1969. Figures 4c-4e show the ensemble mean of the SST anomalies in April 1969 from the hindcast runs with IC only, IC+ENSO forcing, and ENSO forcing only. The shaded areas are with above 95% statistical significance, based on the signal-to-noise ratio estimated from the ensemble mean and the intra-ensemble standard deviation. In the observation, tSA is initially positive while tNA is slightly negative in November 1968. The gradient, G1 = tNA-tSA, is reversed in April 1969 due to the warming in tNA, a canonical response to the positive ENSO forcing from boreal winter to spring (e.g., Huang et al. 2005a). This is captured by the hindcast runs with ENSO+IC (Fig. 4d) and ENSO Only (Fig. 4e). In the IC Only runs (Fig. 4c), the SST anomaly in the South Atlantic in April retains the structure of the initial state in November. However, in North Atlantic, the initial SST anomaly in November decays to nearly zero in April. These results suggest that, in the model runs, tNA in boreal spring was controlled primarily by the ENSO forcing from boreal winter to spring, while tSA was influenced by the persistence of the preconditioning in the preceding winter.

Figure 5 is similar to Fig. 4 but for the 1970-71 case (Figs. 5b-5e are for April 1971), an ENSO cold event in which tNA turned from nearly neutral in November to cold in April (Figs. 5a and 5b). The initially positive tropical Atlantic SST gradient is reversed to negative in spring. This is captured by the hindcast runs with ENSO+IC or ENSO Only, although the model simulations produced too-cold SST anomalies over equatorial Atlantic and tropical South Atlantic. In the IC Only runs, the pattern of SST anomaly in the South Atlantic persisted while that in the tropical North Atlantic dissipated to nearly zero, a behavior similar to the 1968-69 case (Fig. 4c). In the ENSO Only runs, the response in the tropical South Atlantic is very weak. Again, in this case, the simulated tNA is dominated by ENSO forcing while tSA is determined by the persistence of the pre-existing anomaly in winter.

Figure 6 shows the observation and hindcast for the 1982-83 case (Figs. 6b-6e are for April 1983), a strong ENSO warm event. In this case, the response in tNA is canonical; It turns from negative in November (Fig. 6a) to strongly positive in April (Fig. 6b). The close resemblance of Figs. 6d and 6e indicates that the response in spring in the ENSO+IC runs is dominated by the ENSO forcing. In the model, the SST response to ENSO forcing in the equatorial Atlantic and tropical South Atlantic is positive enough (Fig. 6e) to overwhelm a negative SST anomaly from the persistence of the initial condition as inferred from the IC Only runs (Fig. 6c), resulting in a net positive response in the ENSO+IC runs opposite to that observed. Nevertheless, the positive response in tNA is strong enough that the model still predicted a positive G1 in spring, qualitatively consistent with that observed. The errors in the simulated equatorial Atlantic SST could be related to the omission of ocean dynamics in the ocean model. In addition, the excessive warming over the tropical Atlantic in the ENSO+IC and ENSO Only runs may also be attributed in part to the model bias in the atmospheric response to Pacific ENSO forcing. As discussed in Appendix B, the model response in the tropical tropospheric temperature over the Atlantic sector is too strong (too warm during El Niño and too cold during La Niña) compared to observation.

The results for the other three cases are shown in an abridged fashion in Fig. 7 with the left and middle columns the observed SST anomalies in November of yr 0 and April of yr 1, and the right column the simulated SST anomaly in April of yr 1. The hindcast in the right column are from the ENSO+IC runs except for 1993-94 (panel f), which is from the IC Only runs. For the 1988-89 ENSO cold event, the ENSO+IC runs produced the cooling of tNA in spring but not as pronounced as that observed. The simulated SST anomalies in the equatorial and tropical South Atlantic are too cold. This error also occurred in the ENSO Only runs but not in the IC Only runs (not shown), indicating that it is related to the aforementioned model bias in the atmospheric response to ENSO. The model still produced the correct sign (negative) of G1 in boreal spring, due to the simulated substantial cooling in tNA.

The 1993-94 case, middle row of Fig. 7, is unique in that it is an ENSO neutral year with a very strong preconditioning in the Atlantic. Moreover, the observed pattern of the SST anomaly persisted from November 1993 to April 1994 for almost the entire Atlantic domain, preserving the negative G1 from the initial state. The IC Only hindcast runs correctly produced the cool tNA, warm tSA, and negative G1 in boreal spring. Since this is a neutral year, the ENSO+IC runs (not shown) produced similar results as the IC Only runs. With the correct prediction of the tropical Atlantic SST, in Section 4 we will further demonstrate a useful prediction in the precipitation over South America from this case.

For the 1995-96 cold event (bottom row of Fig. 7), the ENSO+IC runs simulated the cooling trend from boreal winter to spring in tNA. The simulated cooling is somewhat excessive, culminating in a negative tNA in April 1996 opposite to that observed. The simulated SST anomalies in spring are also colder than observed for the equatorial Atlantic and tropical South Atlantic. This behavior also exists in the ENSO Only runs (not shown), indicating the influence of the model bias in the ENSO response. Yet, even in this case, the model correctly simulated the sign of G1 (negative) in spring as that observed.

A quick conclusion from the above six cases is that the sign of G1 in boreal spring is not difficult to reproduce in the model simulations. For the ENSO years, this is because the model correctly simulates the warming or cooling in tNA through the robust ENSO-tNA connection. The response in tNA is usually strong enough that, even with some errors in tSA and/or the equatorial Atlantic SST, the sign of G1 in the hindcast can still remain correct. However, the errors in tSA and equatorial Atlantic SST are not without a consequence. We will show in Section 4 that they degrade the prediction of precipitation in some areas in South America.

3b. The evolution of tropical Atlantic SST gradient

The behavior of the monthly mean Atlantic SST gradient, G1, is summarized in Fig. 8 for the (a) 1968-69, (b) 1970-71, and (c) 1993-94 cases. Black, blue, and red indicate the observation and the hindcast runs with ENSO+IC and IC Only, respectively. The half length of the vertical bar indicates one (intra-ensemble) standard deviation. For the 1968-69 warm event with an initially negative G1, without the ENSO forcing the negative G1 persisted into spring (the IC Only runs). The observed upward trend in G1 and the negative value of G1 in spring are correctly simulated with the added ENSO forcing, which dominates in this case. The behavior of the 1970-71 case in Fig. 8b is similar to that of the 1968-69 case but just with a reversal of sign for the SST anomalies; The IC Only runs simulated persistence of a positive G1 into spring, while the ENSO+IC runs correctly produced the downward trend in G1 and a negative G1 in spring as that observed. The behavior of G1 for other ENSO years discussed in Section 3a is qualitatively similar to the above two. For those years, the inclusion of the ENSO forcing is essential for the prediction of G1 in spring.

An intriguing case in which ENSO forcing does not dominate is 1993-94 , shown in Fig. 8c (also see Figs. 7d-7f). Since this is a neutral year, the "ENSO forcing" has only a minor contribution to the prediction of G1 (blue is close to red in Fig. 8c). In the observation (black), an initially strongly negative G1 persisted and maintained its amplitude into spring. The IC Only runs reproduced this persistence although with a greater decay of the amplitude of G1 with time than that observed. Even so, the predicted G1 in April remains strongly negative.

3c. Surface flux response to ENSO forcing

The results of the hindcast experiments may generally depend on the detail of the mixed layer model and the manner of atmosphere-ocean coupling. Although not many ensemble hindcast experiments comparable to ours exist for a clear comparison, we may assess the behavior of our mixed layer model by comparing the ENSO-induced surface fluxes in our coupled model to other studies. Figure 9 shows the effect of the ENSO forcing, defined as the difference between the ensemble means of the ENSO Only and Control runs, on the surface energy fluxes for December-February from ENSO "warm minus cold" composite (see caption for detail). A positive flux anomaly (red) indicates an energy flow into the ocean, corresponding to heating in the SST. The ENSO-induced anomalous latent heat flux (LHF, left) is strongly positive over tNA, the major cause for the warming there from winter to spring. This is consistent with previous studies (e.g., Alexander and Scott 2002). In the Northern Hemisphere, the anomalous long wave (LW, middle) and short wave (SW, right) radiative fluxes as responses to ENSO forcing are generally weaker than the anomalous LHF. There is also a tendency for the LW and SW contributions to cancel each other. Over the African coastal regions, the relatively large values of LW and SW might be related to the variation in cloudiness. The behavior of the anomalous SW and LW radiation in Fig. 9 is somewhat different from that in Alexander and Scott (2002, using a more sophisticated mixed layer model with vertical variations), in which the ENSO forcing induces a positive signal in SW and a moderately negative signal in LW over the tNA region and the Caribbean. In our simulation, the response in the sensible heat flux is weaker than in the other three components and is not shown.

Figure 9 also shows that the ENSO-induced surface energy flux anomalies are generally stronger in the North than in the South Atlantic. This is broadly consistent with the previous argument (e.g., Chang et al. 1998) and our results in Section 3a that, in boreal spring, tropical North Atlantic is more strongly influenced by ENSO while South Atlantic is dominated by internal atmosphere-ocean variability.

4. Hindcast of precipitation

Since our study of the Atlantic SST gradient is motivated by its potential influence on the precipitation over northern South America, we will next examine the simulated precipitation anomalies from the hindcast experiments. The interpretation of the simulated precipitation anomalies is complicated by the fact that the ENSO forcing not only indirectly influences South American rainfall by modifying the Atlantic SST gradient but it can also affect the precipitation through a more direct thermodynamical mechanism (e.g., Chiang and Sobel 2002, and further interpretation in Huang et al. 2005b). Briefly, the direct influence is due to (consider an ENSO warm event) the eastward spreading of warm tropospheric air along the equator from the Pacific to the South American and Atlantic sector (Yulaeva and Wallace 1994, Chiang and Sobel 2002). The resulted warmer air aloft causes an increase in the static stability of the atmosphere over northern South America, thereby a suppression of rainfall there. Thus, northern South America is dry during El Niño and wet during La Niña. This mechanism exists in the ENSO+IC and ENSO Only hindcast runs and it is entangled with the effect of the Atlantic SST gradient in determining the precipitation anomalies over South America. Only in the "IC Only" runs can we clearly relate the precipitation anomalies to the Atlantic SST or SST gradient.

Unlike the SST over the coupled domain that is constrained by the flux correction, the model-predicted precipitation has a more noticeable bias over the tropical Atlantic and South America. The bias over this region is a common problem for GCMs (e.g., Biasutti et al. 2006). In boreal spring, our model produced excessive rainfall over the Amazon basin compared to observation (not shown). To reduce the impact of bias, we define the predicted precipitation anomaly as the difference between the ensemble means of the 25-member hindcast runs and that of another set of 25-member "control runs" (instead of the observed climatology) that retain the coupling over the Atlantic but not ENSO forcing nor imposed initial perturbations in the SST.

The observed precipitation anomalies to be used for model validation are constructed from the daily gridded South American precipitation data set of Liebmann and Allured (2005). A quality check is performed to exclude the grid points where too few observations (too few days - usually 10 days as the threshold - per month) are available to robustly defined the climatology and/or monthly mean anomaly for a particular month. They are left blank in the panels for the observation shown in Figs. 10-13. We will discuss only the four most recent cases of our simulations in the post-1980 era, for which the observation of precipitation has the highest quality.

To assess the impacts of the error in the Atlantic SST on the simulated precipitation, we will further compare our results with a set of nine-member "AMIP" runs - atmospheric GCM forced by the observed SST - using a GCM similar to our hindcast model (both are the T42 28-level version of the NCEP atmospheric GCM but the latter is a slightly more recent version). The model output for the AMIP runs is made available to us through the International Research Institute for Climate and Society (IRI) Data Library. For the AMIP runs, the precipitation anomalies are defined as the departure from the long-term mean deduced from the same set of simulations.

Figure 10 shows the precipitation anomalies for April 1983 from the 25-member ensemble means of our hindcast runs with (a) ENSO+IC, (b) ENSO Only, and (c) IC Only, all to be compared to (d) the 9-member ensemble mean of the AMIP runs, and (e) the observation. The ENSO+IC hindcast runs and the AMIP runs both reproduced the typical dryness over northern Brazil for this ENSO warm event. The observed wetness over the northern (north of the equator) South America is partially reproduced by the AMIP runs but is absent in the ENSO+IC runs, which produced wetness further north over the Caribbean. In the above comparison, it should also be noted that the observation in Fig. 10e represents just one realization, in contrast to the ensemble means in Figs. 10a and 10b. The disagreement in the small-scale structures between the model and observation may be due to sampling. For this strong El Niño case, the drying over northern South America is mainly due to the ENSO forcing. The result of the ENSO Only runs (Fig. 10b) is similar to that of the ENSO+IC runs (Fig. 10a). The IC Only runs (Fig. 10c) produced overall a weaker response but it nevertheless captures the drying over Nordeste. The precipitation anomalies in Fig. 10c can be clearly related to the simulated Atlantic SST anomalies (Fig. 6c). The dipole-like structure (that straddles the equator) in the precipitation anomaly corresponds to a northward shift of ITCZ, consistent with a cool tSA and positive G1 in Fig. 6c. Incidentally, the precipitation anomalies over the equatorial Atlantic and the northern tip of South America from the IC Only runs are more consistent with the observation (and AMIP runs) than those from the ENSO+IC or ENSO Only runs. The latter two produced excessive drying centered on the equator (vs. south of the equator in the IC Only runs, AMIP runs, and observation). This is related to the excessive tropical tropospheric warming as the model bias in the response to El Niño (Appendix B). The effect of the bias somewhat diminished the benefit of adding the ENSO forcing to the hindcast runs even though the forcing was shown to help the prediction of tNA. A similar concern about the mixed benefit of the ENSO forcing for the prediction of remote precipitation anomalies in a coupled model was also put forth by Misra and Zhang (2007).

Figure 11 is similar to Fig. 10 but for April 1996 from the 1995-96 case, a cold event. Except for a reversal of sign, the behavior of the observed and simulated precipitation anomalies in this case is similar to that in Fig. 10. The typical wetness over northern Brazil associated with a cold event is observed (Fig. 11e) and simulated by the AMIP runs (Fig. 11d). The wetness is also simulated by the full hindcast (ENSO+IC) runs (Fig. 11a) but it is weaker compared to Figs.

11d and 11e. The IC Only runs (Fig. 11c) also produced wetness over northern Brazil and a hint of dryness over the northern tip of South America similar to that observed. The result from the ENSO Only runs (Fig. 11b) is mixed. Except for a small-scale dry stripe located along the north shore of northern Brazil, the hindcast produced large-scale wetness over most of northern South America. While this is qualitatively a typical response to La Niña, the simulated wetness was too wide-spread, for example the northern tip of South America is wet, opposite to that observed. This may, again, be related to the bias in the model response to ENSO forcing. Figures 11a-11c also demonstrate that linear superposition cannot be applied to the simulated precipitation field; The sum of the outcomes of the ENSO Only and IC Only runs does not equal that of the ENSO +IC runs, due to the nonlinear dependence of precipitation on the SST and atmospheric circulation.

Figure 12 is similar to Fig. 11 but for the neutral year of 1993-94 (shown is April 1994), and only the IC Only hindcast runs are shown in Fig. 12a. The hindcast with only the information of the initial SST anomaly in November 1993 produced realistic features in the precipitation anomaly with wetness over northern Brazil and dryness over the northwestern tip of South America, similar to that observed (Fig. 12b) and simulated by the AMIP runs (Fig. 12c). The wetness over northern Brazil and dryness north of it in Fig. 12a can be clearly related to the warm tNA and cool tSA (and negative G1) in the simulated SST anomalies (Fig. 7f) that also agree with the observations (Fig. 7e).

Figure 13 is similar to Fig. 12 but for the ENSO cold event of 1988-89 (shown is April 1989), a case in which the full ENSO+IC hindcast runs (Fig. 13a) performed poorly in reproducing the observed precipitation anomaly (Fig. 13b) over South America. The AMIP runs (Fig. 13c), on the other hand, reproduced the observed wetness over northern Brazil and dryness over the northwestern tip of South America. As discussed in Section 3a, for this event, although the ENSO forcing in the ENSO+IC runs produced the observed cooling trend in tNA and the correct sign of G1, it also produced excessive and unrealistic cooling in tSA and the equatorial Atlantic - the sign of the SST anomalies there is the opposite of that observed. In this case, the negative impact of the latter is substantial enough to render the simulated precipitation anomalies inaccurate over the aforementioned regions in South America.

Figure 14 shows the root-mean-square error in the model simulated precipitation anomaly for April of year 1 over the pNSA (Northern tropical South America, top panel) and pSSA (Southern tropical South America, bottom panel) regions as indicated by the red boxes in Fig. 13c. The error is calculated from the difference between the ensemble mean of the model simulation and the observation (interpolated onto model grid) at every grid point over land within the box, and is evaluated for the AMIP, ENSO+IC, ENSO Only, and IC Only runs. From left to right are the three individual ENSO cases, their average, and the neutral case of 1994. The error over pSSA is generally smaller than that over pNSA. For all ENSO cases, except pNSA in 1983, the ENSO+IC runs out-perform the ENSO Only runs in predicting the precipitation anomalies in April. This indicates useful predictability of South American rainfall embedded in the Atlantic preconditioning.

As a summary, except for the 1988-89 case, we found that the relatively simple AGCM +ML coupled model qualitatively reproduced the observed dryness or wetness over northern Brazil south of the equator. For the ENSO years, a greater discrepancy in the precipitation anomalies between the hindcast runs with ENSO forcing and the observation or AMIP runs occur over the northern (north of the equator) and equatorial South America and equatorial Atlantic. This error is attributed in part to the model bias in the atmospheric response to Pacific ENSO forcing (Appendix B). Note that this negative impact of the ENSO forcing on the hindcast of South American precipitation does not contradict the positive impact discussed in Section 3 on the correct simulations of the Atlantic SST gradient, G1. As explained before, for ENSO years the success of the latter is mainly due to the ability of the model to simulate tNA through the ENSO-tNA connection. Our results here imply that the precipitation anomalies over the equatorial South America and equatorial Atlantic depend on more than just tNA and/or the sign of G1. Interestingly, the hindcast for the 1993-94 case does not suffer the problem of the biased response to ENSO since it is a neutral year with minimal ENSO forcing. It reproduced both the observed wetness over northern Brazil and the dryness north of it. Moreover, devoid of ENSO forcing, the successful IC Only "hindcast" may be regarded as a true "forecast", since the predictability of the South American precipitation anomalies in April 1994 is entirely embedded in the initial condition of the SST in November 1993.

5. Concluding remarks

Our analyses of the hindcast experiments indicate that, in the cases with a persistent ENSO forcing from boreal winter to spring, the forcing is the dominant factor in determining the evolution of the tropical Atlantic SST gradient, G1, and the sign of G1 in late spring. In the absence of ENSO forcing, the sign of G1 in boreal winter tends to persist into spring such that the preconditioning in the Atlantic SST also provides a non-negligible contribution to the overall value of G1 in spring. This finding confirms the results of previous observational analyses of a primary role of ENSO but a non-negligible secondary role of Atlantic preconditioning in determining G1 in boreal spring for ENSO events -- recall the statistics of two-third concordant vs. one-third discordant in Huang et al. (2005a). In most cases our hindcast runs with ENSO+IC correctly simulated the sign of G1 in late spring. For the ENSO years, this success is mainly due to the correct simulation of tNA due to its clear connection to ENSO forcing.

The majority of our hindcast runs also simulated reasonable precipitation anomalies over northern Brazil south of the equator, although for ENSO years a larger discrepancy is found between the simulated and observed precipitation anomalies over the northern and equatorial South America and equatorial Atlantic. This is attributed in part to the model bias in the atmospheric response to ENSO forcing. For the ENSO events, the ENSO+IC runs generally out-perform the ENSO Only runs in predicting the rainfall anomalies over the northern half of South America, indicating predictability of South American rainfall embedded in the Atlantic preconditioning. While there is still room for improvement for our model given its biased response to ENSO forcing, the results of this study at least demonstrated that a correct simulation of tNA and the sign of G1 alone does not sufficiently lead to an accurate simulation of the rainfall anomalies over the equatorial South America and the northern South America. The improved simulations for these regions by the AMIP runs indicate that accurate information in tSA and the equatorial Atlantic SST is needed for the prediction of the precipitation anomalies in boreal spring in these regions in South America.

The most interesting case of our numerical experiments is the hindcast (essentially "forecast") for the neutral year of 1993-94, for which the IC Only runs using the observed SST anomaly in November 1993 produced realistic tropical Atlantic SST gradient and precipitation anomalies over northern South America in April 1994. The relationship between the simulated Atlantic SST gradient and South American rainfall anomalies, namely, a negative G1 accompanying the wetness over northern Brazil and the dryness north of it, is consistent with the canonical picture derived from previous observational analyses. The 1993-94 case presents an intriguing example of useful seasonal forecast of G1 and South American rainfall anomalies without ENSO.

Appendix A: Tests for the AGCM+ML model

The mixed layer model consists of a 50 m slab ocean with flux correction. The formula for flux correction follows Peng et al. (2006) but excludes the Ekman transport effect because our desired coupling domain includes the equator (in its vicinity the formula for Ekman transport in Peng et al. (2006) becomes singular). As detailed in Peng et al. (2006), the daily climatology of the SST, T_C, was first constructed from the observation. It was used to force a 60-member ensemble of atmospheric GCM simulations to produce the daily climatology of the (downward) surface heat flux, Q_C. The prognostic equation for the SST in the mixed-layer model can be written in terms of the anomalies of the SST (T) and heat flux (Q),

$$\frac{\partial T'}{\partial t} = \frac{Q'}{(\rho c_p H)} \quad , \qquad \text{(A1)}$$

where $T' = T - T_C$ and $Q' = Q - Q_C$ are the departure from daily climatology, c_p is the heat capacity of sea water, and $H = 50$ m is the depth of the mixed layer. In the coupled model, after (A1) is used to renew T', the total SST is used to force the AGCM. The model is integrated forward to produce the new Q', and so on.

With the constraint of flux correction, the simulated SST does not drift significantly from the climatological seasonal cycle. Figure A1 shows an example of the SST averaged over the South Atlantic box shown in Fig. 1c from a 5-yr test run. Black and red are the observed climatology (repeated for 5 years) and the model simulated SST. The behavior of the simulated

SST over other regions, e.g., the tNA and tSA boxes in Fig. 1a, is similar to that shown in Fig. A1. The climate drift in the SST is generally small during the first 10 months, the duration of our coupled hindcast runs.

We have also performed another set of sensitivity test by extending the northern boundary of the mixed layer model from 36ºN to 50ºN for the 1968-69 case. The simulated tNA, tSA, and G1 in boreal spring are only slightly affected by this change.

Appendix B: Atmospheric response to ENSO forcing in the AGCM+ML model

As noted in Section 3-4, the errors in the hindcast of Atlantic SST may be attributed in part to the model bias related to the atmospheric response to Pacific ENSO forcing. While a comprehensive diagnosis of the model bias is beyond the scope of this study, we will use the 1982-83 case to illustrate an aspect of this bias and its implications for the simulated Atlantic SST. We choose to examine this particular year because it has the strongest Pacific ENSO forcing. Moreover, since the five ENSO warm and cold events we studied each has its own distinctive life cycle (with their maximum SST anomalies peaking at different times), a composite of the five events might not necessarily lead to a clearer picture of the bias.

Figure B1a shows the atmospheric response to the Pacific ENSO forcing in the vertically averaged temperature from our model simulations. The ENSO response is defined as the 25-member ensemble mean of the ENSO-Only runs for 1982-83 minus the 25-member ensemble mean of the control runs (forced by climatological SST), both retain the coupling to the mixed layer model over the Atlantic. The temperature anomaly shown is the average from January-May 1983 and is the mass-weighted vertical average from the surface to $\sigma \approx 0.1$, where $\sigma = p/p_s$ is the terrain-following "sigma" coordinate. Figure B1b is the observational counterpart of B1a, using the sigma-level (spectral coefficient) data from NCEP reanalysis (Kalnay et al. 1996) and with the anomaly defined as the departure from the 1979-2003 climatology. As is well-known, the atmospheric response to a Pacific ENSO SST anomaly generally consists of two components of quasi-stationary wave trains (e.g., Horel and Wallace 1981, Trenberth et al. 1998) and a zonally symmetric response (e.g., Chiang and Sobel 2002, Robinson 2002, Seager et al. 2003). The latter is especially prominent in the tropospheric temperature field, with zonal bands of tropical warming and extratropical cooling accompanying El Niño and the opposite accompanying La Niña (Yulaeva and Wallace 1994, Seager et al. 2003, Chiang and Sobel 2002). In Fig. B1, the zonally symmetric response in the tropospheric temperature is stronger in our simulation than that observed. In the former, the tropical tropospheric warmth spreads eastward more deeply into the Atlantic sector. In the observation, although there is still a positive temperature response on the equator, the temperature anomaly is more confined to the west of the Atlantic sector with the maximum of the temperature anomaly partially blocked by the South American continent. (An examination of the 1995-96 ENSO cold event revealed a similar behavior, namely, in the model the ENSO-induced cold equatorial tropospheric temperature anomaly spreads farther into the Atlantic sector than that observed, causing a cold bias over the equatorial Atlantic, not shown.) Although many factors could potentially contribute to this bias, a plausible one is that the Andes mountain range is severely flattened in the model (due to its relatively coarse T42 resolution), allowing a more thorough eastward intrusion of the tropical tropospheric warm air into the Atlantic sector. The bias discussed here may contribute to the errors in the SST over the equatorial Atlantic and in the precipitation over the equatorial South America and equatorial Atlantic in our hindcast runs with ENSO forcing.

The effect related to the Andes is but one of the plausible explanations for the bias in tropical tropospheric temperature shown in Fig. B1. For example, using the framework of Gill (1980) for the linear response of the tropical atmosphere to an ENSO-like SST forcing, it is known that the ratio of the amplitude of the zonally symmetric to zonally asymmetric temperature response increases with a decreasing damping coefficient (e.g., Gill 1980, Wu et al. 2001, Bretherton and Sobel 2002). The bias of an excessive zonally symmetric warmth induced by El Niño (coolness induced by La Niña) might also arise from too weak effective damping (by parameterized boundary layer friction, cumulus friction, etc.) in the tropics in our model. These possibilities are worth exploring in future work.

Acknowledgment

The authors thank Dr. Brant Liebmann for providing the South American precipitation data set used in this study. This work was supported by NSF grant ATM-05-43256, NOAA CLIVAR-Atlantic Program, NOAA CPPA Program, and the CICAR award No. NA03OAR4320179 from NOAA, U.S. Department of Commerce.

References

Alexander, M., and J. Scott, 2002: The influence of ENSO on air-sea interaction in the Atlantic, *Geophys. Res. Lett*., **29**, 1701, doi:10.1029/2001GL014347

Barreiro, M., A. Giannini, P. Chang, and R. Saravanan, 2004: On the role of the Southern Hemisphere atmospheric circulation in tropical Atlantic variability, in *Earth's Climate: the ocean-atmosphere interaction*, *Geophys. Monogr. Ser*., vol. 147, edited by C. Wang, S.-P. Xie, and J. Carton, pp. 143-156, AGU, Washington, D. C.

Bretherton, C. S., and A. H. Sobel, 2003: The Gill model and the weak temperature gradient approximation, *J. Atmos. Sci.*, **60**, 451-460

Biasutti, M., A. H. Sobel, and Y. Kushnir, 2006: AGCM precipitation biases in the tropical Atlantic, *J. Climate*, **19**, 935-958

Chang, P., L. Ji, H. Li, C. Penland, and L. Matrosova, 1998: Prediction of tropical Atlantic sea surface temperature, *Geophys. Res. Lett.*, **25**, 1193-1196

Chiang, J. C. H., and A. H. Sobel, 2002: Tropical tropospheric temperature variations caused by ENSO and their influence on the remote tropical climate, *J. Climate*, 15, 2616-2631

Czaja, A., P. van der Vaart, and J. Marshall, 2002: A diagnostic study of the role of remote forcing in tropical Atlantic variability, *J. Climate*, **15**, 3280-3290

Enfield, D. B., and D. A. Mayer, 1997: Tropical Atlantic sea surface temperature variability and its relation to El Nino-Southern Oscillation, *J. Geophys. Res.*, **102**, 929-945

Giannini, A., R. Saravanan, and P. Chang, 2004: The preconditioning role of tropical Atlantic variability in the development of the ENSO teleconnection: implications for the prediction of Nordeste rainfall, *Clim. Dynam.*, **22**, 839-855

Gill, A. E., 1980: Some simple solutions for heat-induced tropical circulation, *Q. J. R. Meteor. Soc.*, **106**, 447-462

Horel, J. D., and J. M. Wallace, 1981: Planetary-scale atmospheric phenomena associated with the Southern Oscillation, *Mon. Weather Rev.*, **109**, 813-829

Huang, H.-P., A. W. Robertson, and Y. Kushnir, 2005a: Atlantic SST gradient and the influence of ENSO, *Geophys. Res. Lett.*, **32**, L20706, doi:10.1029/2005GL023944

Huang, H.-P., R. Seager, and Y. Kushnir, 2005b: The 1976/77 transition in precipitation over the Americas and the influence of tropical sea surface temperature, *Clim. Dynam.*, **24**, 721-740

Kalnay, E., and co-authors, 1996: The NCEP/NCAR 40-year reanalysis project, *Bull. Am.*

Meteorol. Soc., **77**, 437-471

Liebmann, B., and D. Allured, 2005: Daily precipitation grids for South America, *Bull. Am. Meteor. Soc.*, **86**, 1567-1570

Misra, V., and Y. Zhang, 2007: The fidelity of NCEP CFS seasonal hindcasts over Nordeste, *Mon. Weather Rev.*, **135**, 618-627

Nobre, C. A., and L. C. B. Molion, 1988: The climatology of droughts and drought prediction, in "The impact of climate variations on agriculture: Assessments in semi-arid regions", M. Parry, T. R. Carter, and N. T. konjin, Eds., Kluwer Academic, pp. 305-323

Peng, S., W. A. Robinson, S. Li, M. A. Alexander, 2006: Effects of Ekman transport on the NAO response to tropical Atlantic SST anomaly, *J. Climate*, 19, 4803-4818

Robinson, W. A., 2002: On the midlatitude thermal response to tropical warmth, *Geophys. Res. Lett.*, **29**, doi:10.1029/2001GL014158

Saravanan, R., and P. Chang, 2004: Thermodynamic coupling and predictability of tropical sea surface temperature , in *Earth's Climate: the ocean-atmosphere interaction*, *Geophys. Monogr. Ser.*, vol. 147, edited by C. Wang, S.-P. Xie, and J. Carton, pp. 171-180, AGU, Washington, D. C.

Seager, R., N. Harnik, Y. Kushnir, W. Robinson, J. Miller, 2003: Mechanisms of hemispherically symmetric climate variability, *J. Climate*, **16**, 2960-2978

Trenberth, K. E., G. W. Branstator, D. Karoly, A. Kumar, N.-C. Lau, and C. Ropelewski, 1998: Progress during TOGA in understanding and modeling global teleconnections associated with tropical sea surface temperature, *J. Geophys. Res.*, **103**, 14291-14324

Trzaska, S., A. W. Robertson, J. D. Farrara, and C. R. Mechoso, 2007: South Atlantic variability arising from air-sea coupling: local mechanisms and tropical-subtropical interactions, *J. Climate*, **20**, 3345-3365

Uvo, C. B., C. A. Repelli, S. E. Zebiak, and Y. Kushnir, 1998: The relationship between tropical Pacific and Atlantic SST and northeast Brazil monthly precipitation, *J. Climate*, **11**, 551-562

Wu, Z., E. S. Sarachik, and D. S. Battisti, 2001: Thermally driven tropical circulations under Rayleigh friction and Newtonian cooling, *J. Atmos. Sci*., **58**, 724-741

Yulaeva, E., and J. M. Wallace, 1994: The signature of ENSO in global temperature and precipitation fields derived from the microwave sounding unit, *J. Climate*, **7**, 1719-1736

Figure captions

Fig. 1 The composites of the March-May SST anomalies for the (a) concordant, and (b) discordant, cases for all major ENSO warm events from 1865-2000. A concordant case is defined as the one in which the tropical Atlantic SST gradient, G1, in March-May has the same sign as the NINO3 index in the preceding December-January. A discordant case is the opposite. The composite of the SST anomalies in January-March, i.e., precursor to the SST anomaly in Fig. 1b, for the discordant cases is shown in (c). The two boxes in (a) are the regions used to define tNA and tSA. Contour interval is 0.1C, negative dashed. Shading indicates a high level (> 95%) of statistical significance. Adapted from Huang et al. (2005).

Fig. 2 The observed monthly-mean tropical Atlantic SST index, G1 (right), and the NINO3 SST index (left panel) for 1948-1997. Each row is a year, defined as July of yr 0 to June of yr 1. The top row is for July 1947-June 1948 and bottom row July 1996-June 1997. The years indicated by an arrow are selected for our hindcast experiments. The year indicated at right corresponds to year 1. The color scales are shown at bottom. Note that the color interval for G1 is one-third of that for NINO3.

Fig. 3 A test run for illustrating the behavior of the hindcast model. Shown are the simulated daily surface temperature anomalies averaged over the South Atlantic box in Fig. 1c for the ensemble mean (black) and the individual ensemble members (colored lines) for a set of 3-member runs. The initial SST perturbation, imposed to the mixed layer model at November 1 of year 0 (when the coupling is turned on), is constructed from the composite of the average of the October and November monthly SST anomalies from 1953, 1959, 1969, 1974, 1983, 1988, and 1994. The selected years satisfy the criterion that the SSTA of (October+November)/2 averaged over the South Atlantic box is greater than 0.3C. The filled and open circles are the simulated (ensemble mean) and observed (composite of the six selected years) monthly SSTA for the South Atlantic box.

Fig. 4 The SST anomalies for the 1968-69 case. (a) Observed SSTA in November of yr 0

(1968). (b) Observed SSTA in April of yr 1 (1969). (c)-(e) The 25-member ensemble means of the model simulated SSTA with IC Only (c), ENSO+IC (d), and ENSO Only (e) (See text for detail). Shading indicates a high level (> 95%, using the ensemble mean anomaly and intra-ensemble variance to define the signal-to-noise ratio) of statistical significance.

Fig. 5 Same as Fig. 4 but for the 1970-71 case.

Fig. 6 Same as Fig. 4 but for the 1982-83 case.

Fig. 7 Similar to Fig. 4 but for, top to bottom, 1988-89, 1993-94, and 1995-96. The left column shows the observed SSTA in November of yr 0, middle column the observed SSTA in April of yr 1, and right column the simulated SSTA from the hindcast experiments. For the 1988-89 (panel c) and 1995-96 (panel i) cases the ENSO+IC runs are shown. For the 1993-94 case, an ENSO neutral year, the IC Only runs are shown in the right column.

Fig. 8 The observed (black) and model simulated (blue with ENSO+IC, red with IC only) monthly mean G1 for (a) 1968-69, (b) 1970-71, and (c) 1993-94.

Fig. 9 The ENSO-induced anomalies in the surface latent heat flux (left), long wave radiative energy flux (middle), and short wave radiative energy flux (right panel) averaged from December of year 0 to February of year 1 and defined as the difference between the ensemble means of the ENSO-Only and Control runs. Shown is the ENSO warm minus cold composite, defined as the average of the two warm events (1968-69, 1982-83) minus the average of the three cold events (1970-71, 1988-89, 1995-96). Red (positive) means a net energy flux into the ocean, corresponding to heating in the SST.

Fig. 10 The precipitation anomalies for April 1983. (a) Hindcast with ENSO+IC. (b) Hindcast with ENSO Only. (c) Hindcast with IC Only. (d) AMIP runs. (e) Observation. (a)-(c) are 25-member ensemble means from the 1982-83 case. (d) is the 9-member ensemble mean. Color scale is shown at bottom.

Fig. 11 Same as Fig. 10 but for April 1996 (hindcast runs for the 1995-96 case). (a) ENSO+IC. (b) ENSO Only. (c) IC Only. (d) AMIP runs. (e) Observation.

Fig. 12 The precipitation anomalies for April 1994. (a) Hindcast with IC Only. (b) Observation. (c) AMIP runs.

Fig. 13 Same as Fig. 12 but for April 1989 (hindcast runs for the 1988-89 case). In panel (c), the red boxes north and south of the equator over South America indicate the pNSA and pSSA regions, respectively, used for Fig. 14.

Fig. 14 The root-mean-square error in the precipitation anomaly for April of year 1 averaged over the pNSA (top panel) and pSSA (bottom panel) regions as defined in Fig. 13c. The error is calculated from the r.m.s. of the ensemble mean of the hindcast minus observation at every grid point over land within the box. The errors associated with the AMIP, ENSO+IC, ENSO-Only, and IC-Only runs are shown in green, red, blue, and gray. The three groups of bars at left are for the three individual post-1980 ENSO events discussed in the text. The group marked by "AVE" is the average over the three events. The error for the neutral year 1994 is shown at right.

Fig. A1 The SST averaged over the South Atlantic box in Fig. 1c from observation (black, with repeated seasonal cycle) and a 5-yr test run of the AGCM+ML model (red).

Fig. B1 (a) The model simulated response to the tropical Pacific ENSO forcing in the vertically averaged temperature, defined as the mass-weighted average of temperature from the surface to $\sigma \approx 0.1$, where σ is the terrain-following "sigma" coordinate. Shown is the temperature anomaly averaged from January-May 1983. (b) The observational counterpart of (a), constructed from sigma-level temperature data from NCEP reanalysis. Contour interval is 0.2°C. Red and blue are positive and negative, respectively. Areas with the absolute value of the temperature anomaly less than 0.2°C are not colored.

Table 1. Summary of the major hindcast runs performed for this study. Each case, indicated by a tick mark, consists of 25 one-year runs from September of year 0 to August of year 1 and with coupling to the mixed layer model over the Atlantic switched on at November 1 of year 0. The ENSO warm and cold events are indicated at right.

	ENSO-Only	ENSO+IC	IC-Only	No ENSO, No IC	Remark
1968-89	√	√	√		Warm
1970-71	√	√	√		Cold
1982-83	√	√	√		Warm
1988-89	√	√	√		Cold
1993-94		√	√		Neutral
1995-96	√	√	√		Cold
Control				√	

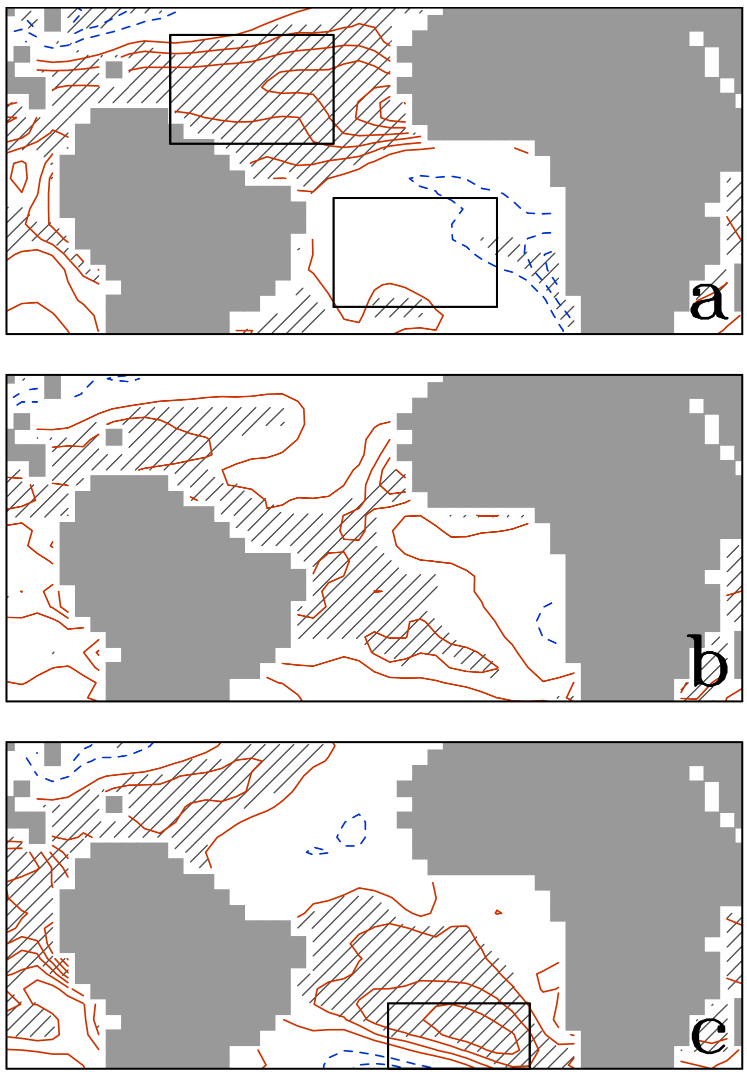

Fig. 1

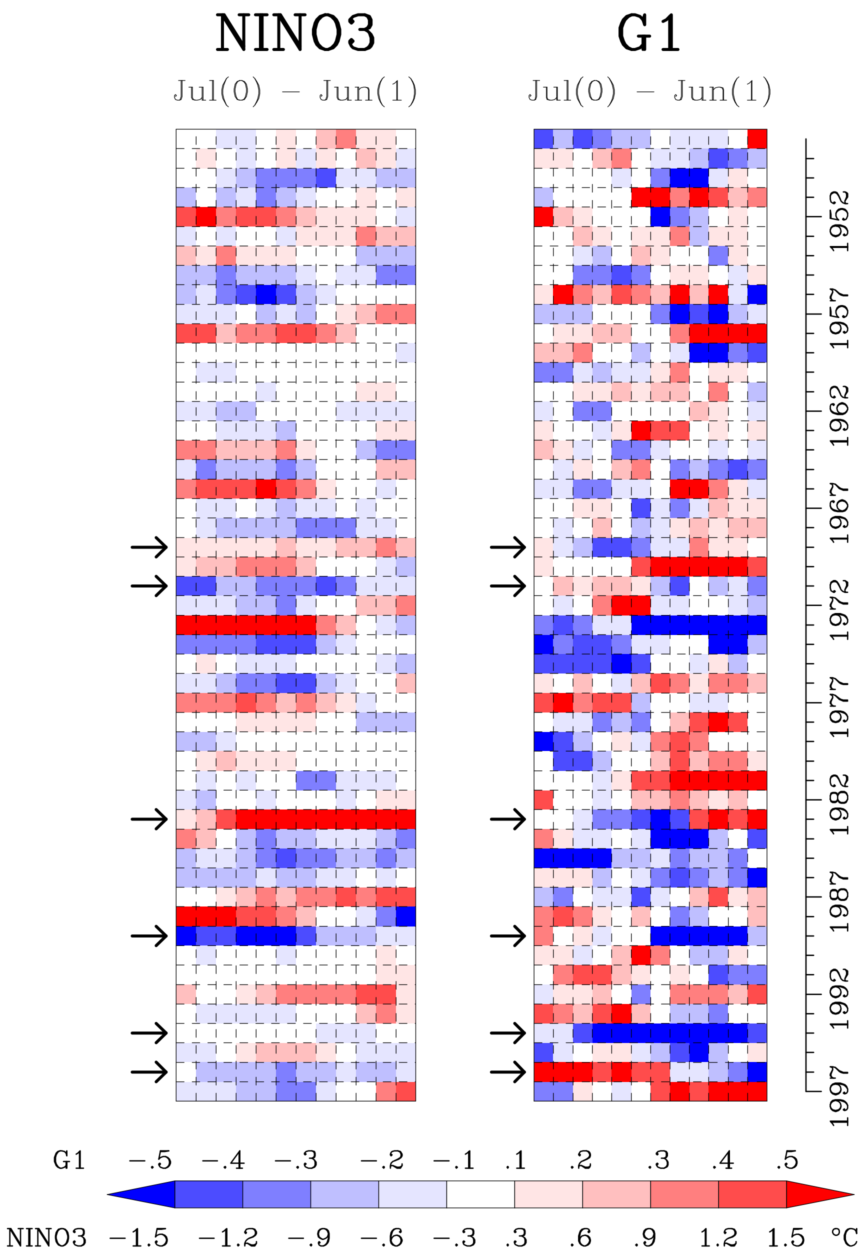
NINO3
Jul(0) – Jun(1)
G1
Jul(0) – Jun(1)
1952
1957
1962
1967
1972
1977
1982
1987
1992
1997
G1 −.5 −.4 −.3 −.2 −.1 .1 .2 .3 .4 .5
NINO3 −1.5 −1.2 −.9 −.6 −.3 .3 .6 .9 1.2 1.5 °C

Fig. 2

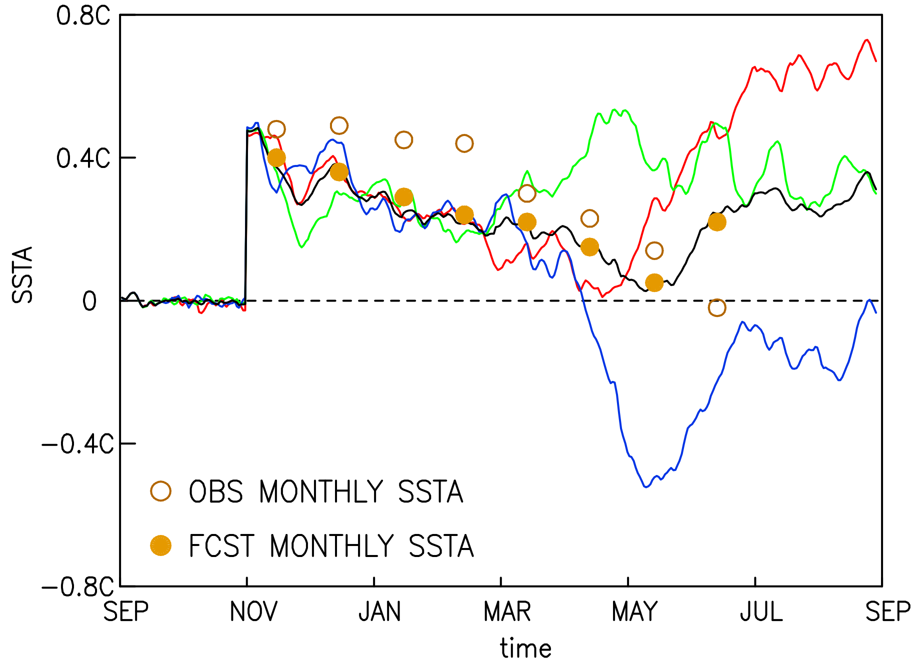
0.8C
0.4C
0
−0.4C
−0.8C
SSTA
OBS MONTHLY SSTA
FCST MONTHLY SSTA
SEP
NOV
JAN
MAR
MAY
JUL
SEP
time

Fig. 3

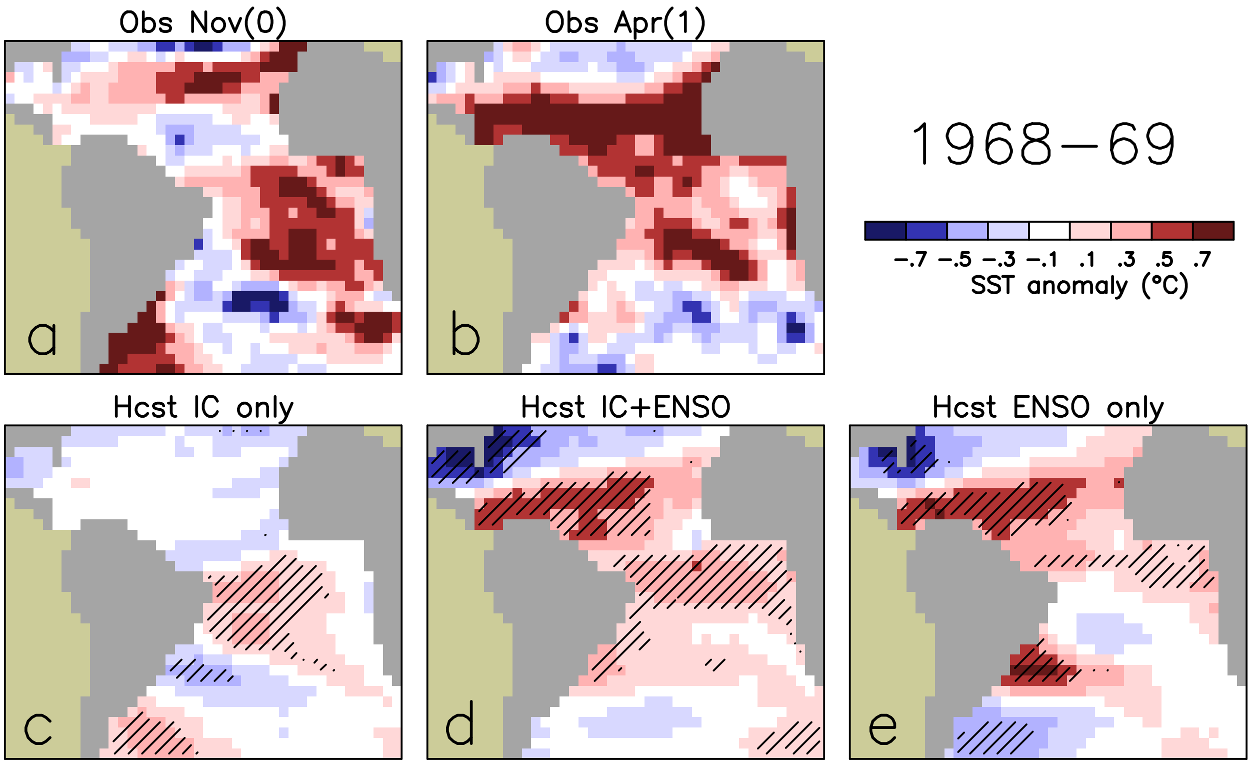
Obs Nov(0)
Obs Apr(1)
1968−69
−.7 −.5 −.3 −.1 .1 .3 .5 .7
SST anomaly (°C)
Hcst IC only
Hcst IC+ENSO
Hcst ENSO only
a
b
c
d
e

Fig. 4

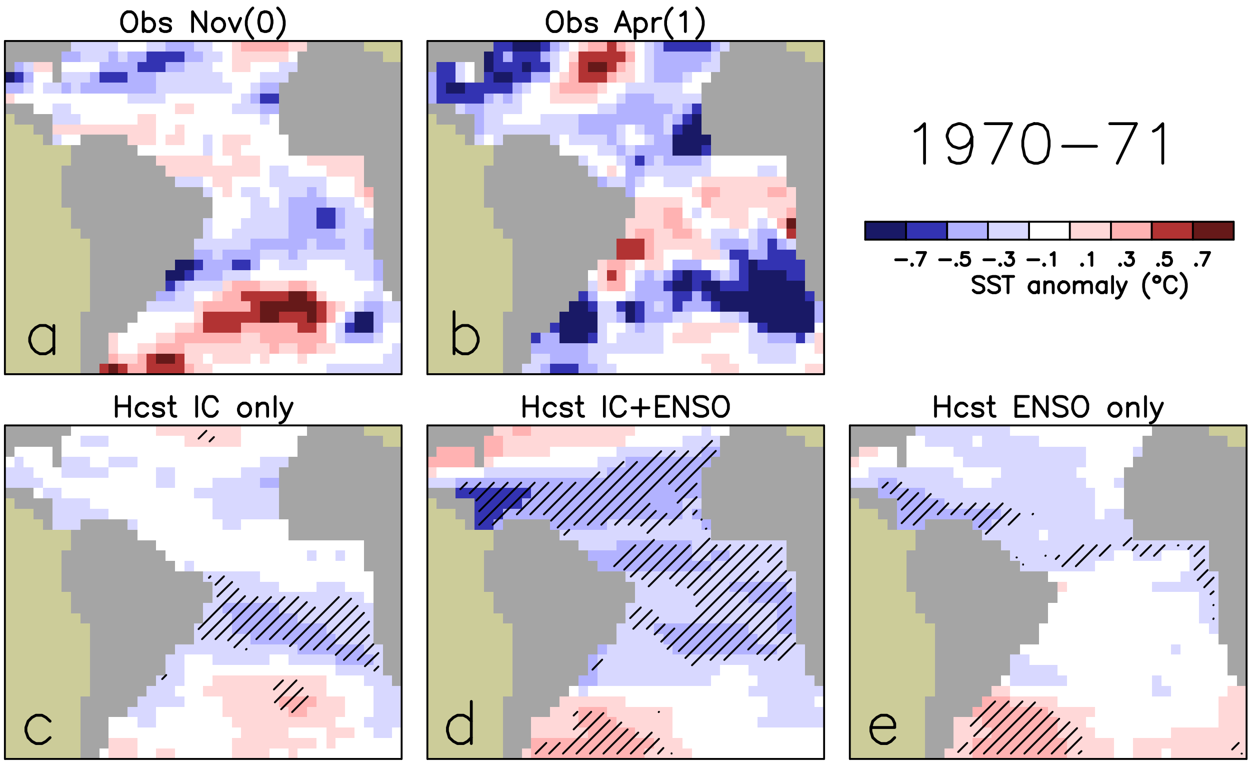
Obs Nov(0)
Obs Apr(1)
1970−71
−.7 −.5 −.3 −.1 .1 .3 .5 .7
SST anomaly (°C)
a
b
Hcst IC only
Hcst IC+ENSO
Hcst ENSO only
c
d
e

Fig. 5

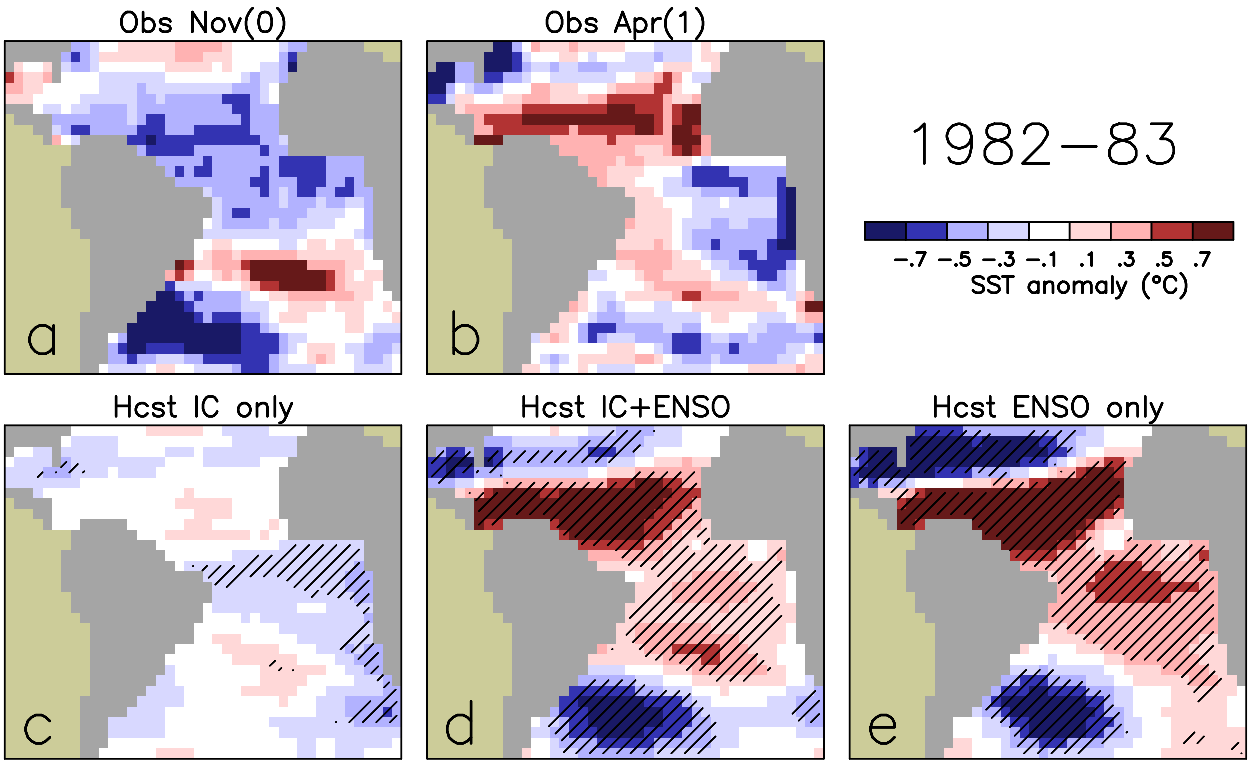

Obs Nov(0)
a
Obs Apr(1)
b
1982−83
−.7 −.5 −.3 −.1 .1 .3 .5 .7
SST anomaly (°C)
Hcst IC only
c
Hcst IC+ENSO
d
Hcst ENSO only
e

Fig. 6

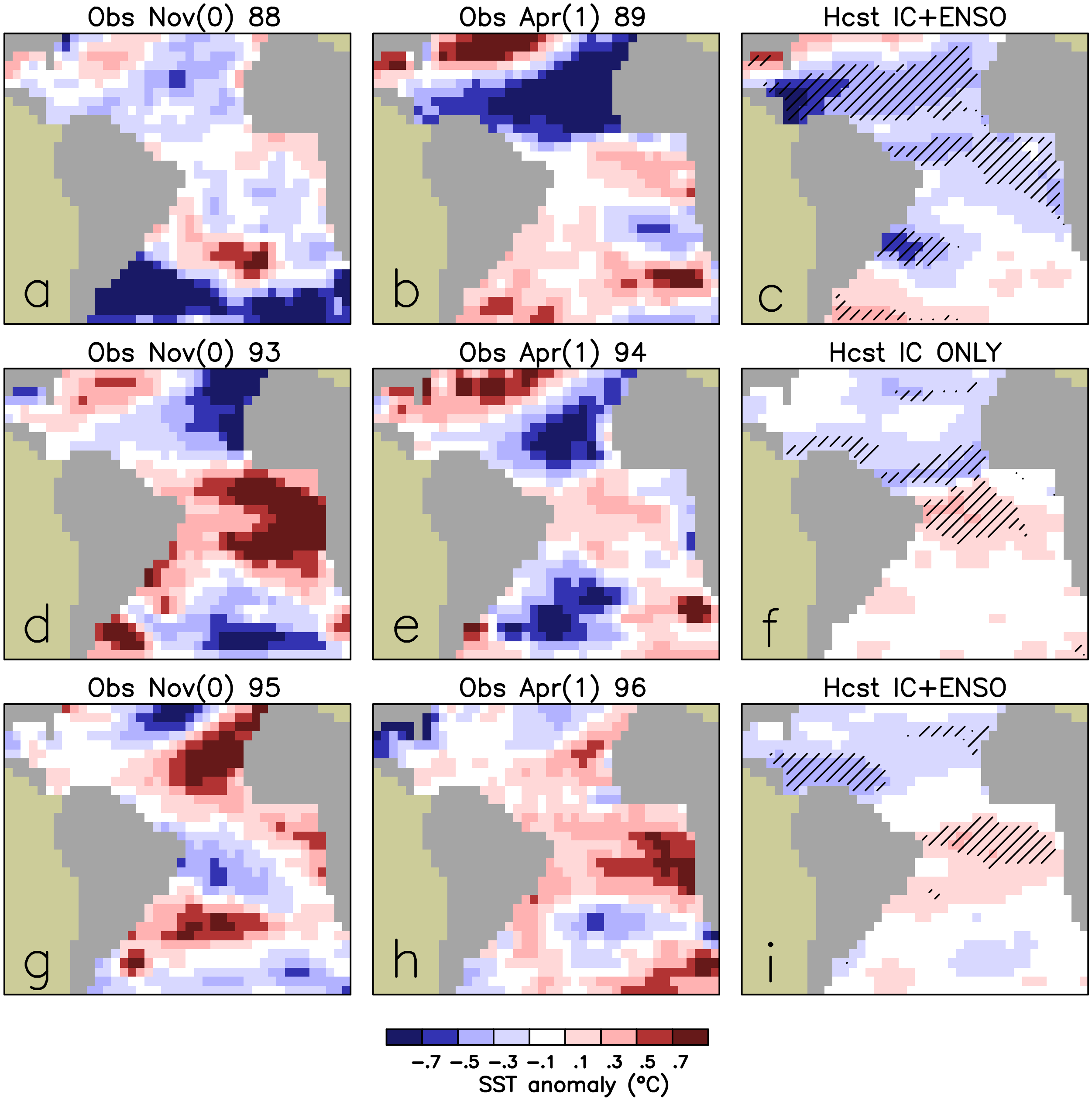

Obs Nov(0) 88
Obs Apr(1) 89
Hcst IC+ENSO
a
b
c
Obs Nov(0) 93
Obs Apr(1) 94
Hcst IC ONLY
d
e
f
Obs Nov(0) 95
Obs Apr(1) 96
Hcst IC+ENSO
g
h
i
−.7 −.5 −.3 −.1 .1 .3 .5 .7
SST anomaly (°C)

Fig. 7

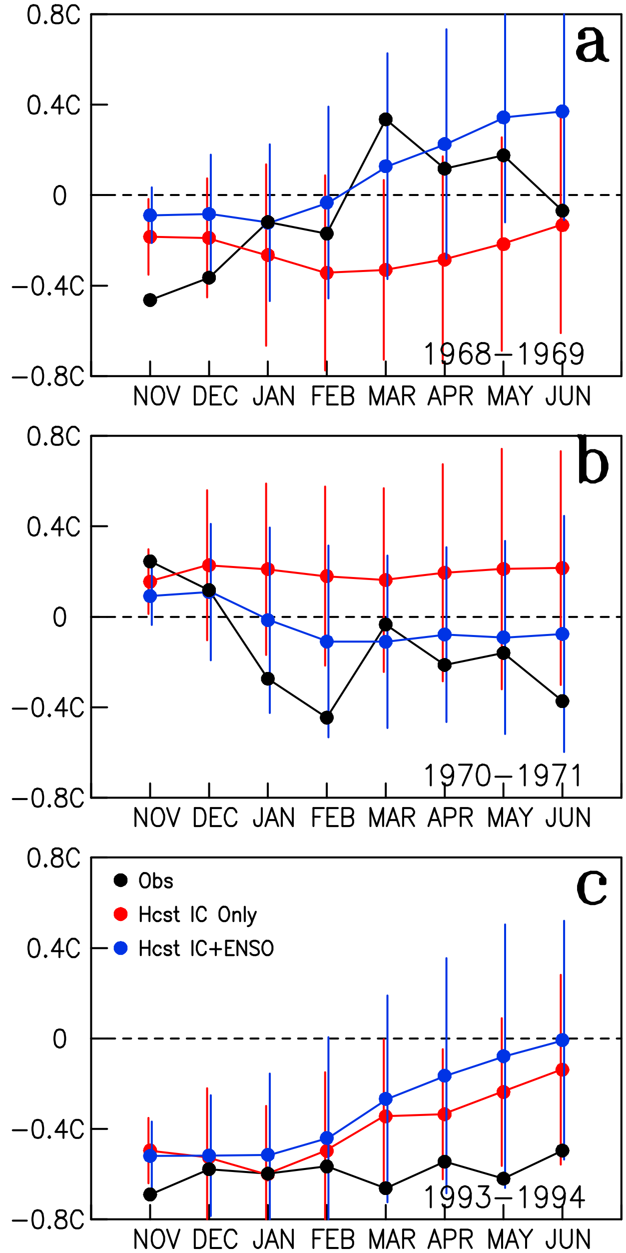
0.8C
0.4C
0
−0.4C
−0.8C
a
1968−1969
NOV DEC JAN FEB MAR APR MAY JUN
b
1970−1971
c
Obs
Hcst IC Only
Hcst IC+ENSO
1993−1994

Fig. 8

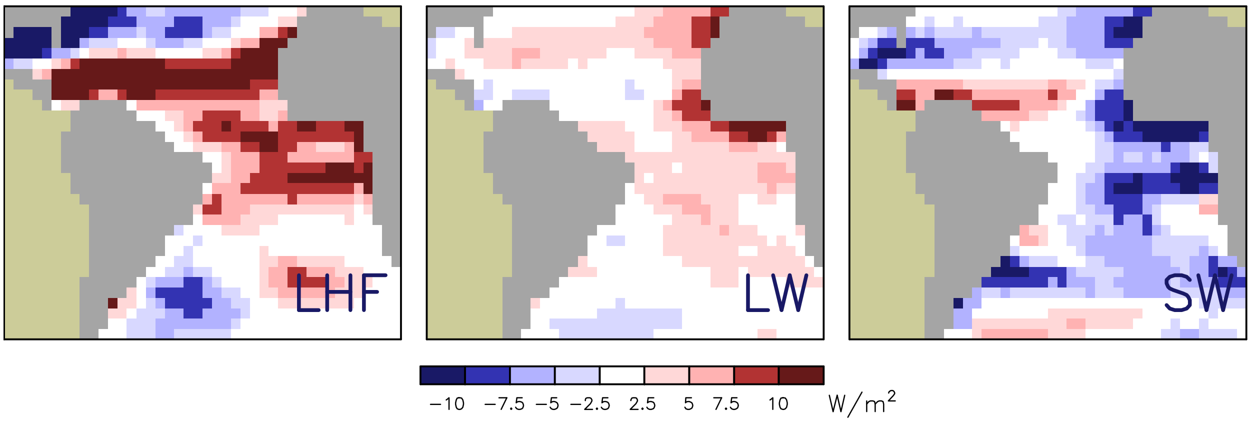

Fig. 9

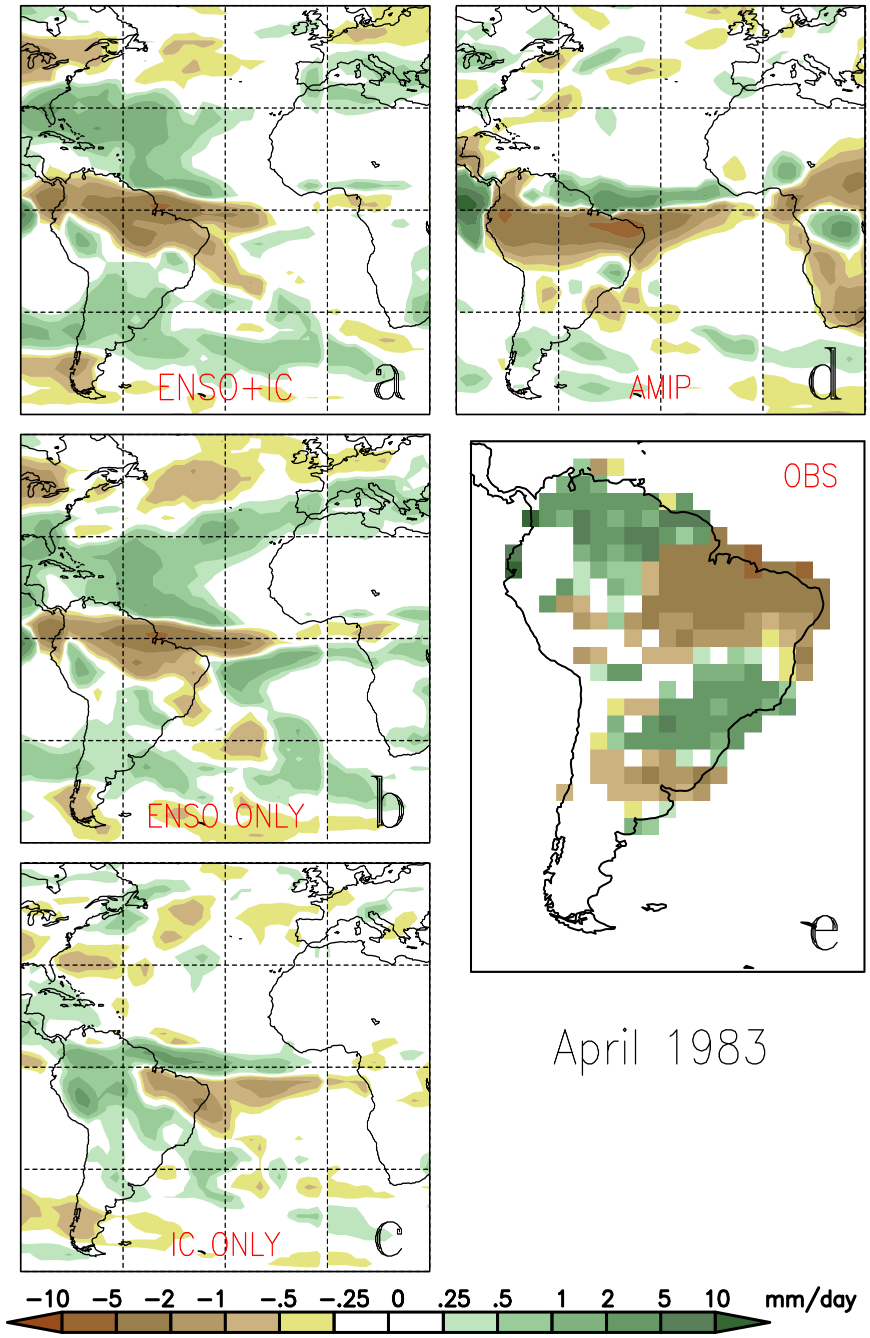
ENSO+IC
a
AMIP
d
ENSO ONLY
b
OBS
e
IC ONLY
c
April 1983
−10 −5 −2 −1 −.5 −.25 0 .25 .5 1 2 5 10 mm/day

Fig. 10

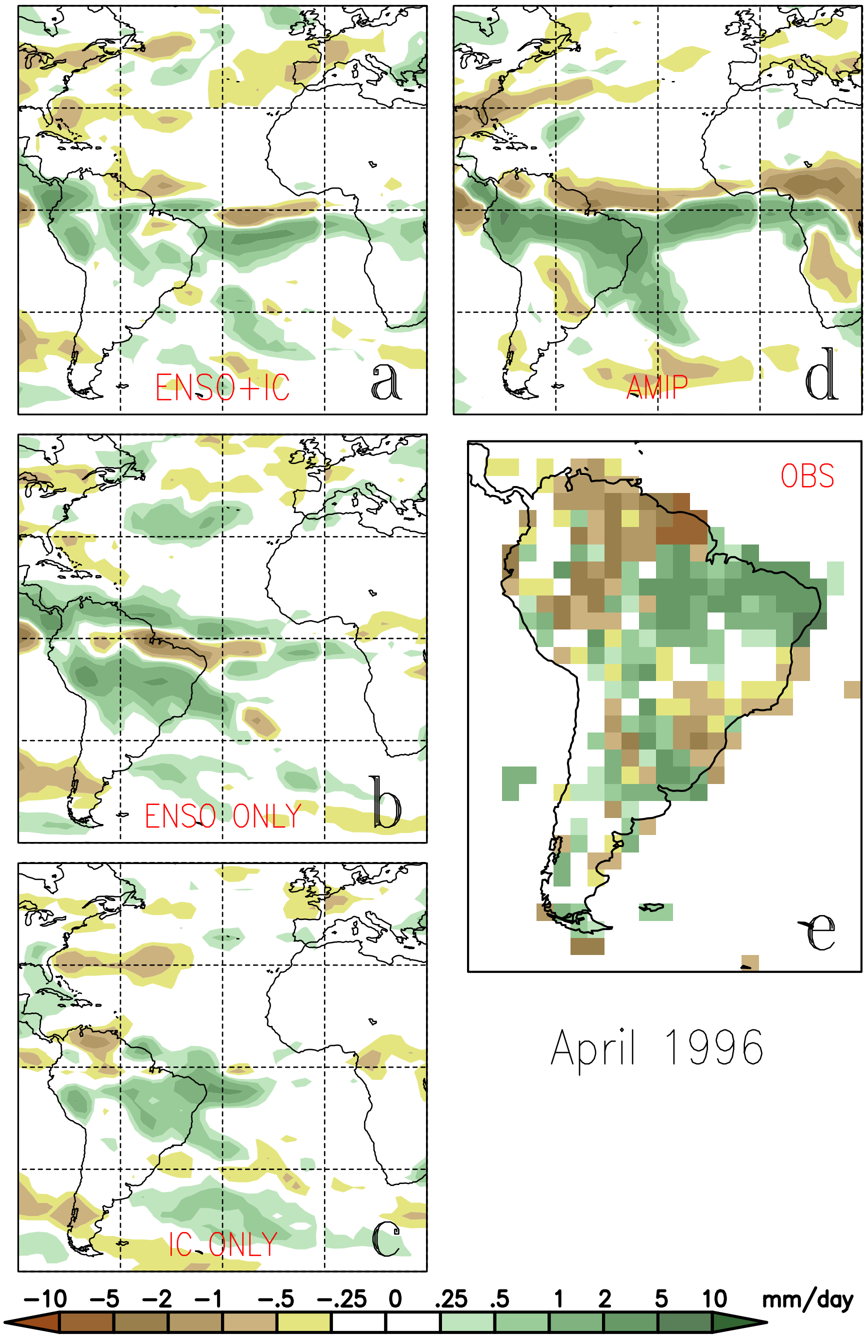
ENSO+IC
a
AMIP
d
ENSO ONLY
b
OBS
e
IC ONLY
c
April 1996
−10 −5 −2 −1 −.5 −.25 0 .25 .5 1 2 5 10 mm/day

Fig. 11

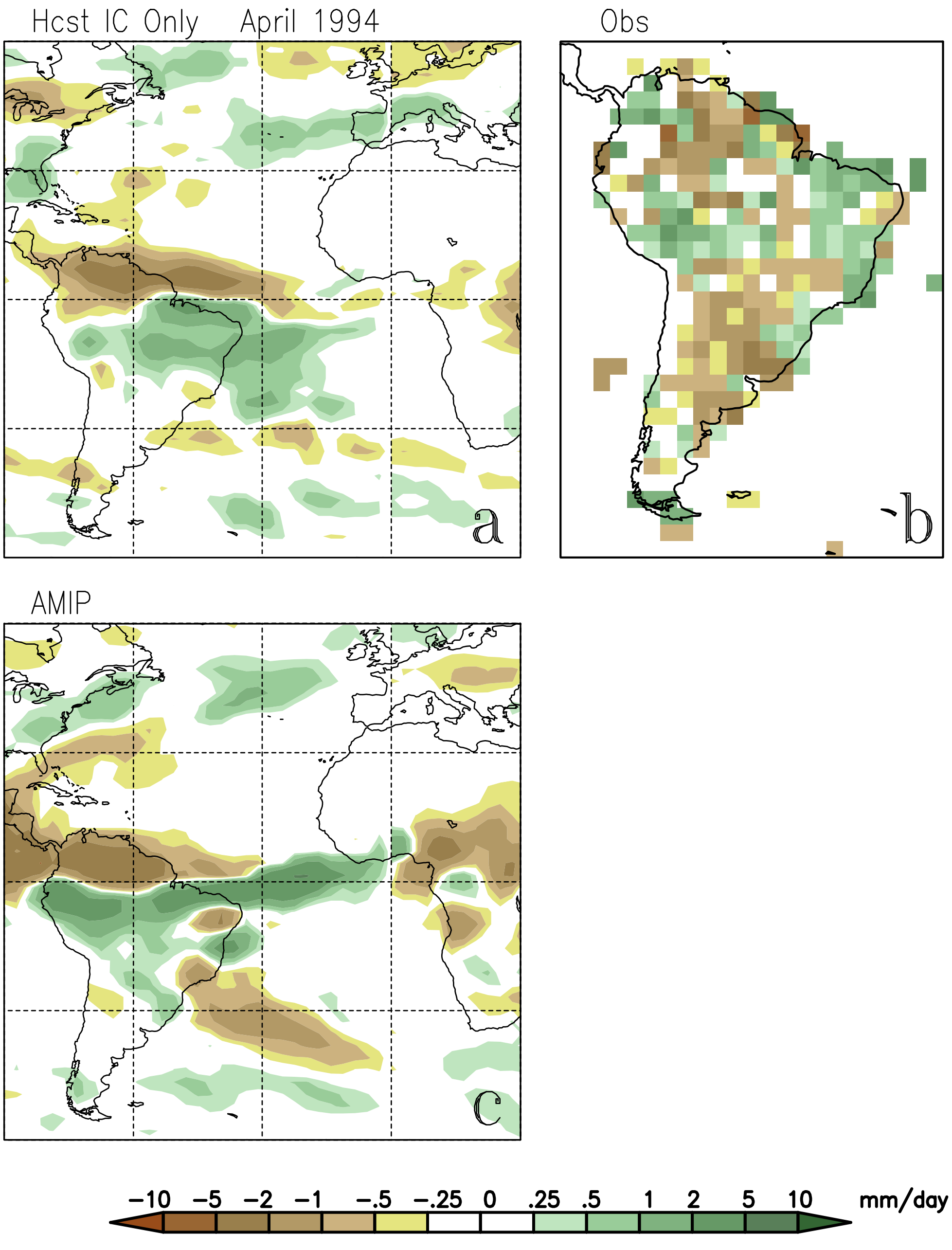
Hcst IC Only April 1994
Obs
a
b
AMIP
c
−10 −5 −2 −1 −.5 −.25 0 .25 .5 1 2 5 10
mm/day

Fig. 12

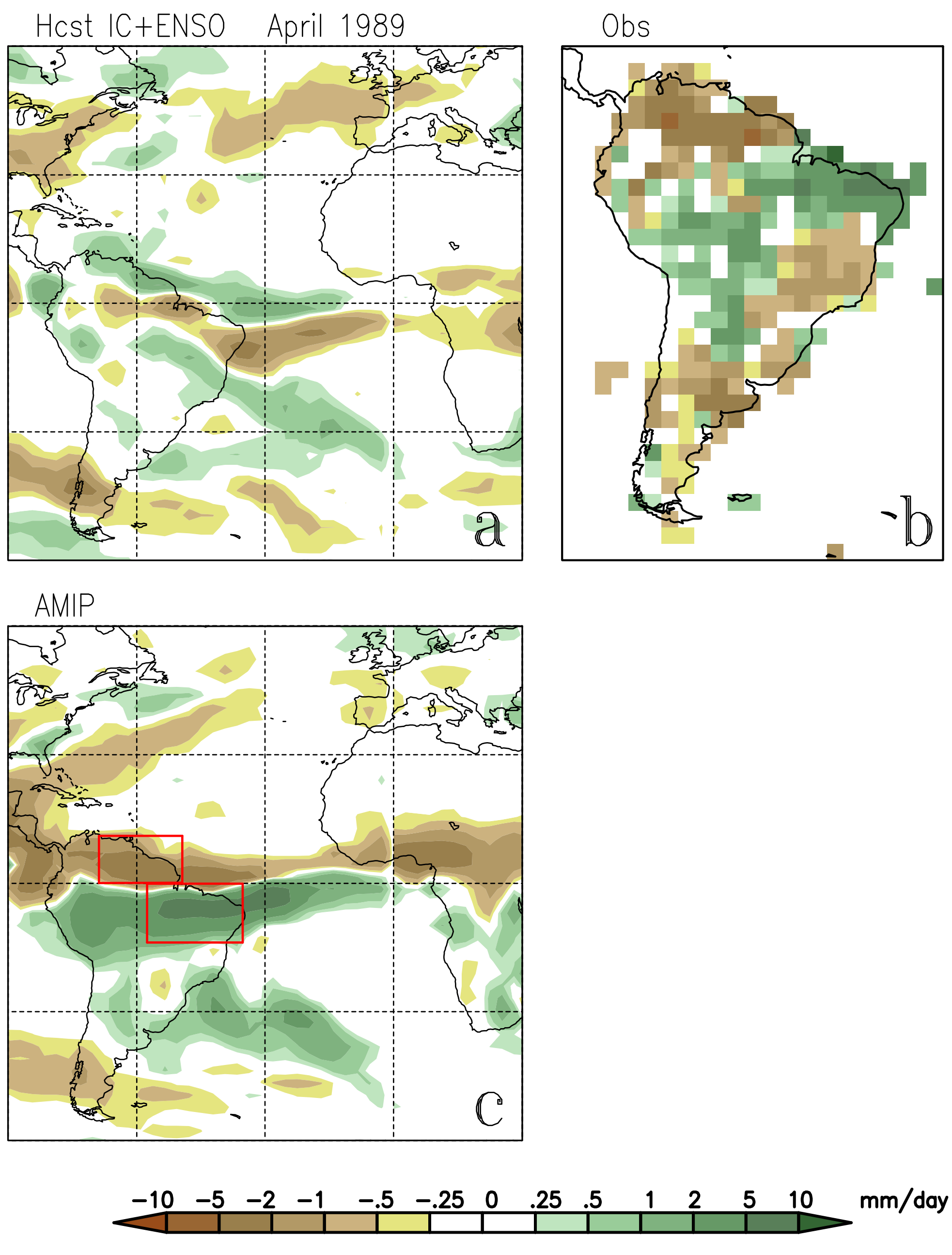

Hcst IC+ENSO April 1989
Obs
a
b
AMIP
c
−10 −5 −2 −1 −.5 −.25 0 .25 .5 1 2 5 10 mm/day

Fig. 13

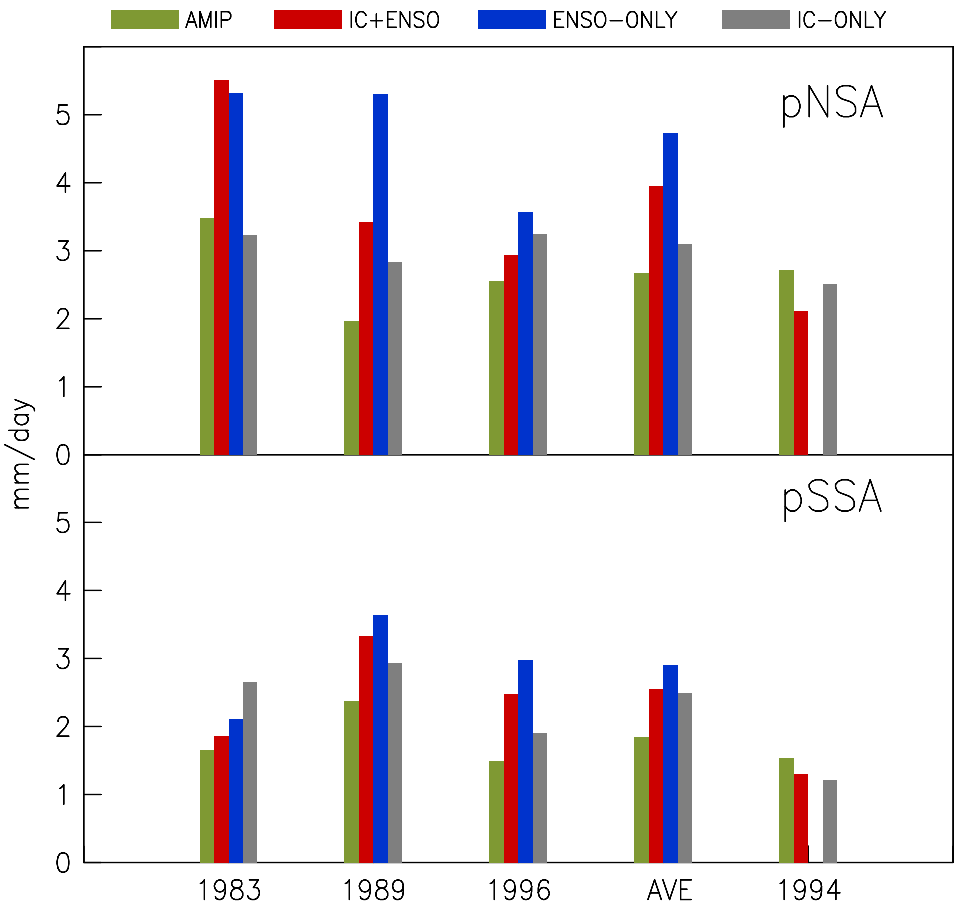
AMIP
IC+ENSO
ENSO-ONLY
IC-ONLY
pNSA
pSSA
mm/day
0
1
2
3
4
5
1983
1989
1996
AVE
1994

Fig. 14

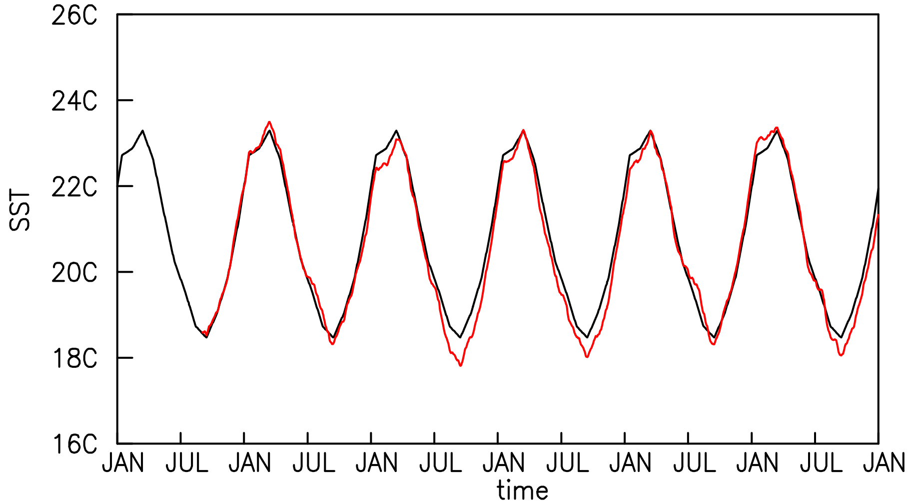
26C
24C
22C
20C
18C
16C
SST
JAN
JUL
JAN
JUL
JAN
JUL
JAN
JUL
JAN
JUL
JAN
JUL
JAN
time

Fig. A1

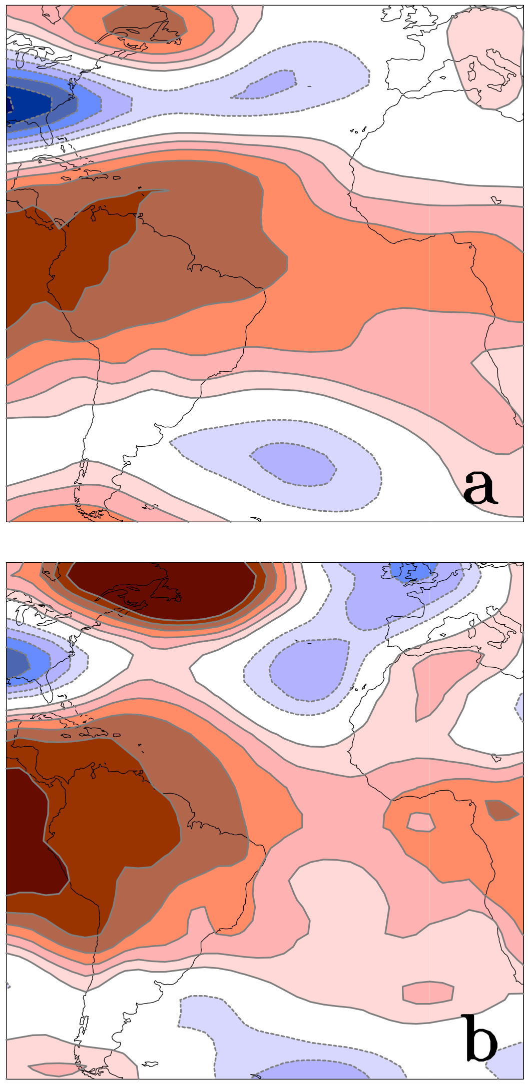

Fig. B1